JST: Smart Systems and Devices
Volume 35, Issue 1, January 2025, 040-047

A Self-Locking Electrostatic Microgripper

Nguyen Ngoc Minh, Phuc Hong Pham*
Hanoi University of Science and Technology, Ha Noi, Vietnam
**Corresponding author email: phuc.phamhong@hust.edu.vn*

Abstract

The paper presents design, calculation, and simulation of a novel electrostatically actuated microgripper with a self-locking mechanism. The working principle of the electrostatic comb-drive actuator (ECA) is based on the tangential electrostatic force when applying a voltage between two capacitors. The microgripper is driven by lateral comb-drive actuators with a maximum displacement which can be up to 40μm at the calculated voltage of 110.06 volt. Additionally, the self-locking mechanism which consists of two V-beams and ratchet racks at both sides will help the gripping jaws grip, lock and move micro samples without driving voltage. Both analytical calculation and finite element analysis (FEA) were performed to verify the advantages of the proposed design as well as test the maximum stress of the elastic components. Results show that both calculation and simulation displacement are quite close with the average deviation of 0.3%. The maximum error is approximately 1.23% at the driving voltage of 100 volts.

Keywords: Microgripper, electrostatic comb-drive actuator (ECA), self-locking mechanism, finite element analysis (FEA).

1. Introduction

Microgrippers are the typical components of Micro-Electro-Mechanical-Systems (MEMS). They were designed to grasp, hold, and manipulate micro-objects in micro/nano scale. The microgrippers are often integrated into microsystems for applications in micro-robotics, micro-assembly, microsurgery or endoscopy, etc. In addition, micro grippers act as end-effectors for the pick-and-place operation of micro-particles in material science or biology. It is an efficient device for operating in a very small workspace with different environments such as air, liquids, or vacuum sites [1]. In the past decades, there were a lot of microgrippers that have been developed for various applications which generally can be classified based on driving physics effects. Shape memory alloys (SMA) [2], piezoelectric [3], electrothermal [4], and electrostatic [5] actuation systems are frequently used as mechanisms for grasping micro-objects. Among these, the electrostatic actuator has some advantages: high working stability at room temperature, high-frequency response (up to hundreds of kHz under resonance), and the lowest power consumption. The electrostatic effect used for microgripper is based on the principle of the electrostatic comb-drive actuator developed by W.C. Tang *et al*. in 1990 [6]. The comb-drive actuator requires simple fabrication technology that is fully Integrated Circuits (IC) processing compatibility. Furthermore, since most living objects such as cells and bacteria cannot sustain high temperature and large force that are typical for electrothermal actuators, electrostatic microgrippers are a great selection in bio-micromanipulation [7] or medicine [8].

According to the movement configurations, there are two main types of electrostatic actuation: lateral and perpendicular comb-drive actuators. The difference between these types is the direction of the actuating force, which are tangential and normal electrostatic forces, respectively. The perpendicular comb-drive actuators, because of the nonlinear relationship between the force generated and finger gaps, the difficulty of controlling the force produced, will be not suitable for applying in microgrippers [9]. On the other hand, the lateral comb-drive is the most popular actuator for microgrippers due to its linear driving force and easier to control.

Recently, some MEMS microgrippers with different advantages have been designed for applications in microscale. For example, a 2-DOF microgripper that can provide movements along both *x*- and *y*-axes was reported in [10]. A rotary microgripper using a divider circuit to increase the linearity of electrostatic force [11]. The electrostatic microgripper using amplification mechanism to obtain a large displacement [12]. Or an active released-object mechanism used for microgripper to overcome adhesion force [13]. Nevertheless, their feature requires a constant voltage supply during the process of gripping, which may damage the micro-objects, especially living objects like cells. In [14],

ISSN 2734-9373
https://doi.org/10.51316/jst.179.ssad.2025.35.1.5
Received: Aug 14, 2024; revised: Oct 14, 2024;
accepted: Oct 31, 2024

a microgripper with a post-assembly self-locking mechanism was designed to solve the problem. It can grip any micro-objects with size from 0 to 100 µm and only needs a driving signal during gripping and releasing micro-objects steps. However, the self-locking mechanism involves a complex post-assembly process structure, which can make the fabrication and assembly process more challenging.

In this paper, we propose a novel microgripper integrating self-locking mechanism that helps it grip and move micro-objects without driving voltage. The self-locking mechanism with a quite simple design allows easily grasping and releasing the sample. In addition, each of the two arms is actuated independently, as well as generating relatively larger gripping range.

2. Configuration and Calculation of the Microgripper

2.1. Design and Working Principles

Fig. 1 shows the configuration of the microgripper. The working principle of microgripper is based on the horizontal movement of parallel capacitors (i.e. movable comb fingers) connected to anchors ①. The shuttles ④ are connected to the gripper arms ⑤ at one side, the other side of the gripper arms are connected to four S-shaped springs ⑥ and the self-locking mechanism ⑦. These springs are used to push the gripping arm returning to the initial position.

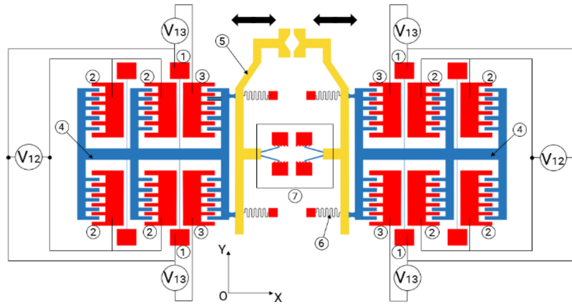

Fig. 1. Schematic view of the microgripper

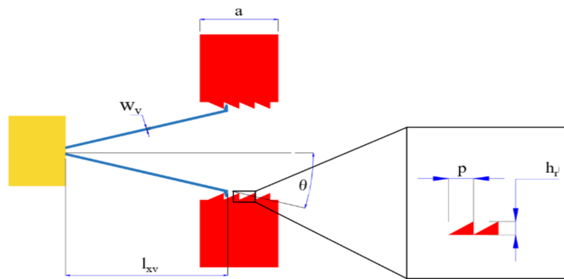

Fig. 2. Configuration of self-locking structure

When applying a DC voltage (V_{12}) between fixed electrodes ② and movable comb fingers ①, the electrostatic force generated between the electrodes will push the shuttle ④ as well as the gripping arm ⑤ moving forward in *X*-direction. The tip of *V*-beams of the self-locking mechanism ⑦ will move inside and slide on the surface of static ratchet teeth (Fig. 2). The ratchet mechanism helps to keep the *V*-beams (i.e. gripping arms) cannot move backward if the tip of *V*-beams overcomes each pitch p of ratchet tooth. In other words, the ratchet mechanism supports the gripping arms to grasp micro sample without applying voltage V_{12}.

To unlock and release the micro sample, a DC voltage V_{13} is applied between the electrodes ① and ③ for both sides. The shuttle ④ and gripping arm ⑤ will move backward in *X*-direction (due to the electrostatic force as well as elastic force of springs ⑥) and release the micro sample. Here, both electrostatic and spring forces will support the *V*-beams sliding and moving to the original position.

In this structure, the outstanding feature of the microgripper is to grasp and self-lock the sample with various diameters due to ratchet mechanism and without clamping voltage (see Fig. 2). It is to help save energy consumption of the system.

Table 1: Structure parameters of the comb-drive actuator and the self-locking mechanism

Parameter	Symbol	Value	Unit
Width of the V-beam	w_v	3	µm
Length of the V-beam in X-direction	l_{xv}	200	µm
Slope angle of the V-beam with respect to X-direction	θ	15	°
Width of ratchet rack anchors	a	100	µm
Pitch of ratchet tooth	p	8	µm
Height of ratchet tooth	h_r	5	µm
Length of a single finger	L_0	50	µm
Gap between two comb fingers	g_0	2	µm
Number of movable fingers on each comb-drive actuator	n	380	
Width of a single finger	w_0	3	µm
Thickness of the device layer	b	30	µm
Length of an elastic beam	L	600	µm
Width of an elastic beam	w	5	µm
Number of the flexure beam on each actuator	n_b	4	
Cover width of springs	L_1	100	µm
Width of spring cross-section	w_1	2.5	µm
Radius of spring curved paths	R	10	µm
Number of S-shaped of spring turns	i	10	

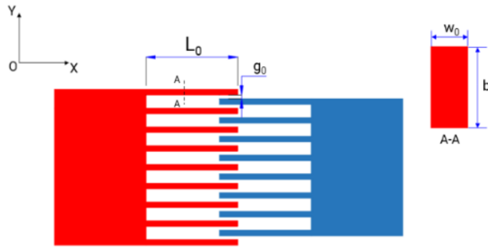

Fig. 3. Configuration of the comb fingers

The geometrical dimensions of the ECA as well as its components are shown in Fig. 3 and Table 1, in which n is total number of the movable fingers for gripping phase; L_0, b, w_0 is the length, thickness and width of single finger, respectively; g_0 is the gap between two comb fingers.

2.2. Displacement of Gripping Jaw

When applying a voltage V_{12}, the electrostatic force is generated to produce a linear motion. The tangential electrostatic force can be calculated as follows:

$$F_e = \frac{nb\varepsilon\varepsilon_0 V^2}{g_0} \tag{1}$$

where n = 380 is total number of movable fingers on each comb-drive actuator; $\varepsilon_0 = 8.854 \times 10^{-12}$ (F/m) and $\varepsilon = 1$ are permittivities of vacuum and air, respectively; $g_0 = 2\mu m$ is the gap between two fingers; $b = 30\mu m$ is the thickness of the comb finger.

Considering the force acting on one gripper arm, we have the equilibrium equation of force in X-direction as follows (see Fig. 7a later below):

$$F_e - F_b - F_d - 2F_{spr} = 0 \tag{2}$$

F_b is the total elastic force of the actuator's beam:

$$F_b = K_b \Delta x \tag{3}$$

where Δx is the displacement of the comb fingers or of the gripping jaw in X-direction; K_b is the stiffness of the beam system, with two pairs of beams: $u = n_b/2 = 2$, we have:

$$K_b = \frac{24u\mathrm{EI}}{L^3} = \frac{4\mathrm{E}bw^3}{L^3} \tag{4}$$

here, E = 169 GPa is the Young's modulus of the silicon, w equals 5μm is the width of the elastic beam, L equals 600 μm is the length of each beam (Table 1).

The hindering forces act on the self-locking mechanism following (Fig. 4): F_a is the elastic force of V-beams (perpendicular to length l of V-beam), F_a' is obtained by project F_a onto Y-directions, N is the normal force perpendicular to the inclined surface of ratchet tooth, F_{fr} is the frictional force between the tip of V-beam and surface of the ratchet tooth, F_d is the total hindering force in X-direction caused by the frictional forces.

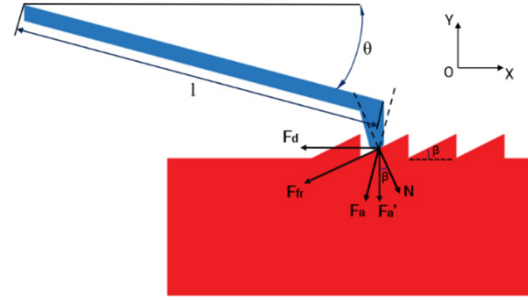

Fig. 4. Force analysis acting on the self-locking mechanism.

These forces can be calculated as follows:

$$F_a' = \frac{3\mathrm{EI}_1}{l^3} cos\theta \Delta y \tag{5}$$

$$N = F_a' cos\beta \tag{6}$$

$$F_{fr} = f_m N \tag{7}$$

$$F_d = 2F_{fr} cos\beta \tag{8}$$

where $\beta = 31.97^0$ is the slope angle of the ratchet tooth. I_1 and l are the inertia moment and the length of the V-beam, respectively ($l = l_{xv}/\cos\theta$); θ equals 15^0 is the slope angle of the V-beam with respect to the horizontal direction; Δy is the displacement of the tip of the V-beam in Y-direction (changing from 0 to 5μm); f_m equals 0.3 is the frictional coefficient between the silicon-silicon contact surface [15].

F_{spr} is the elastic force of the springs and can be calculated as:

$$F_{spr} = K_{spr} \Delta x \tag{9}$$

To obtain the stiffness of the spring ⑥, the deformation simulation under a specified load was performed in ANSYS. With a loading force of 50μN, the maximum simulating deformation was 30.546μm, i.e. the stiffness of each spring K_{spr} is 1.637(μN/μm) (Fig. 5b). The dimensions of spring are also shown in Fig. 5a and Table 1.

From (2) to (9), we can obtain the relation between the displacement Δx of the gripping jaw and applied voltage V_{12}:

$$\Delta x = \frac{\left(\frac{nb\varepsilon\varepsilon_0 V^2}{g_0} - 2f_m \frac{3EI_1}{l^3} cos\theta\, cos^2\beta \Delta y\right)}{\left(\frac{4Ebw^3}{L^3} + 2K_{spr}\right)} \tag{10}$$

To guarantee the operation of the self-locking mechanism, the displacement Δx of gripper jaw must be larger or equal the pitch p of ratchet tooth:

$$\Delta x \geq p = 8(\mu m) \tag{11}$$

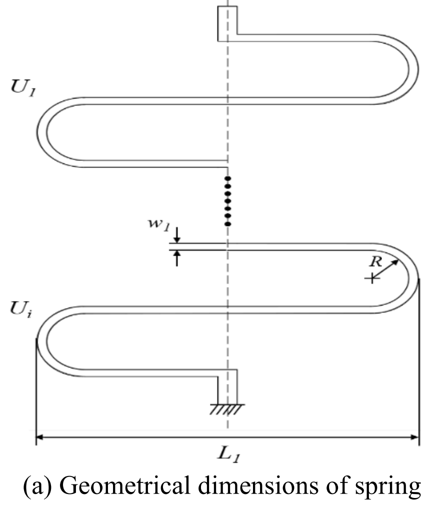

(a) Geometrical dimensions of spring

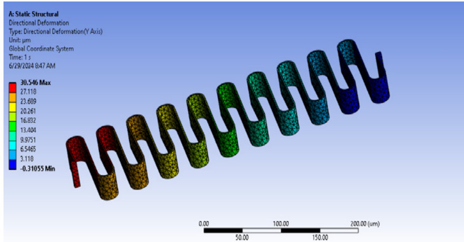

(b) Simulation of spring

Fig. 5. Configuration and simulation of spring

From equations (9) and (10), the driving voltage V_{12} must satisfy a condition as below:

$$V \geq \sqrt{\frac{g_0\left[\left(\frac{4Ebw^3}{L^3} + 2K_{spr}\right)\Delta x + 2f_m \frac{3EI_1}{l^3} cos\theta cos^2\beta\Delta y\right]}{nb\varepsilon\varepsilon_0}} \quad (12)$$

or:

$$V_{min} = \sqrt{\frac{g_0\left[\left(\frac{4Ebw^3}{L^3} + 2K_{spr}\right)\Delta x + 2f_m \frac{3EI_1}{l^3} cos\theta cos^2\beta\Delta y\right]}{nb\varepsilon\varepsilon_0}} \quad (13)$$

Therefore, from (13), the minimum driving voltage can be expressed as:

$$V_{min} = 50.4\ (V) \quad (14)$$

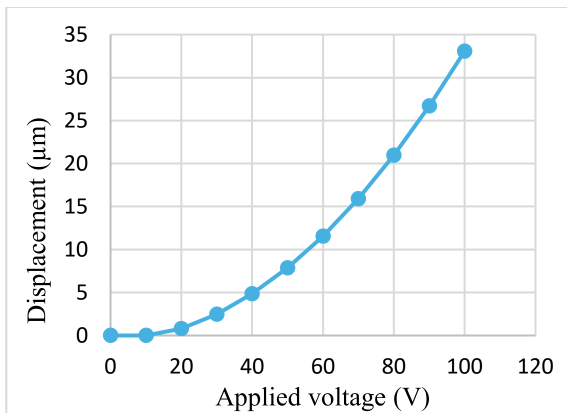

Fig. 6. The relationship between displacement and applied voltage

2.3. Gripping Force and the Voltage Condition for Gripping Sample

This section determines the relationship between gripping force F_k generated on each jaw and the driving voltage V when gripping the sample with a specific mass and size.

To determine the relationship between the driving voltage and the gripping force, we assume the micro sample is a cylinder (Fig. 7b) with the height H and the diameter d. Fig. 7a shows the diagram of the force acting on gripping arm and the sample. Here, F_p is the driving force from the shuttle acting on the grip-arm, F_{ct} is the gripping force at points M and M' in the jaw. These forces can be calculated as:

$$F_p = F_e - F_b - F_d - 2F_{spr} \quad (15)$$

By solving (15), the gripping force F_p ensuring the jaw touching the sample will be determined. However, this force is not enough for the gripper to grip and lift the sample at the same time. We need to increase the total force F_p to overcome the weight of the sample.

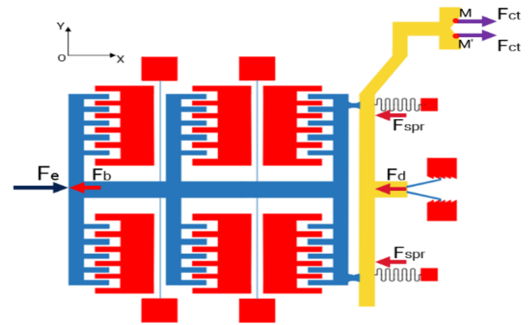

(a) Force analysis on the half of gripper

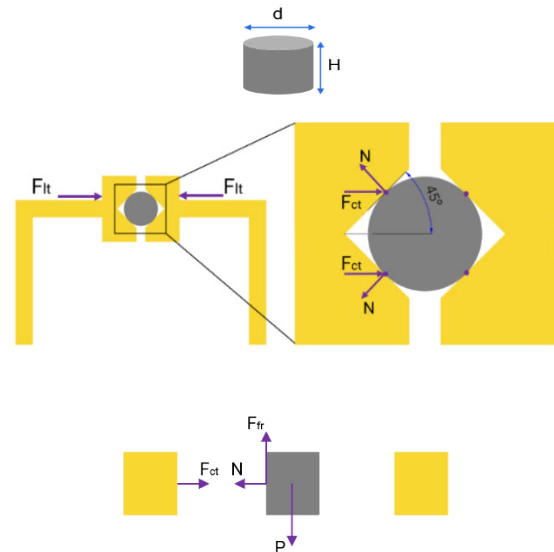

(b) Force acting on the micro sample

Fig. 7. Force analysis on the half of gripper (a); and on the gripped sample (b)

In other words, the frictional forces F_{fr} exerted by two jaws must be greater than the weight P of the sample (Fig. 7b).

$$4F_{fr} \geq P \quad (16)$$

$$F_{ct} = N\cos(45^0) = \frac{P}{4f_m}\cos(45^0) = \frac{mG}{4f_m}\cos(45^0) = \frac{\pi d^2 H\rho}{16f_m} G\cos(45^0) \quad (17)$$

$$F_{lt} = 2F_{ct} \quad (18)$$

Here, F_{lt} is the force so that the gripper can lift the sample. Assume that H equals 40µm is height of the sample; ρ equals 2330 kg/m^3 is the density of the silicon; G equals 9.81m/s^2 is gravitational acceleration; d is the diameter of the sample. The minimum gripping force F_k that grip and lift the sample is calculated as:

$$F_k = F_p + F_{lt} \quad (19)$$

From (15) to (19), the relation between the driving voltage V and the sample's diameter d is illustrated in Fig. 8.

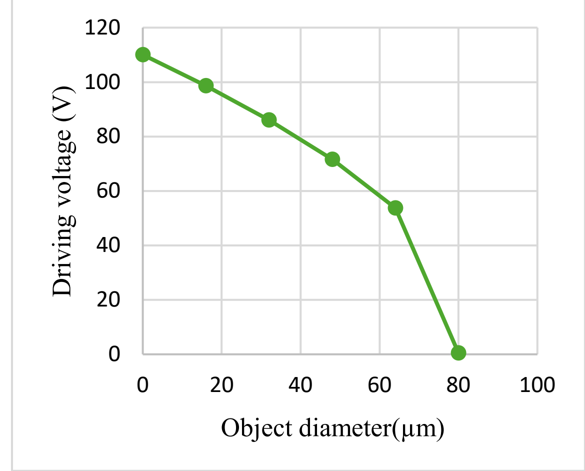

Fig. 8. The relationship between driving voltage and the diameter of the sample

2.4. Voltage for Returning Period

When applying a voltage V_{13} for two actuators nearest gripping jaws (see Fig. 1), the electrostatic force F_e' is generated to produce a returning motion of ECA as well as of the V-beams. In this case, the electrostatic force F_e' can be calculated using (1) with the number of movable fingers n' = 250 for release phase. With the support of S-shaped spring forces and of actuator's beams, the total returning force in X-direction will be:

$$F_{re} = F_e' + 2F_{spr} + F_b \quad (20)$$

The returning force acts on each side of V-beam can be expressed as:

$$F'_{re} = \frac{F_{re}}{2} \quad (21)$$

The returning condition is that the free end of V-beam is bended by the moment M at the distance s equals 15µm (see Fig. 9):

$$M = F'_{re}.s \quad (22)$$

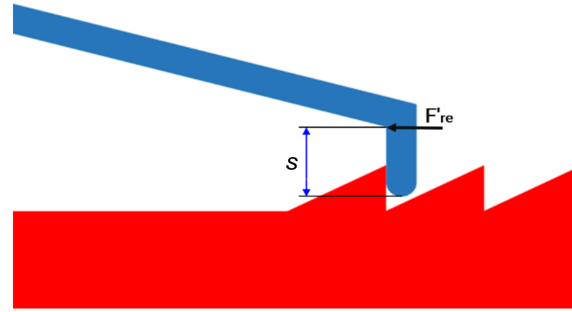

Fig. 9. Force acts on the free end of V-beam in returning period

Considering the free end of V-beam as a cantilever beam with the fixed region at the contact area with the ratchet tooth (Fig. 10a). Here, $F_{critical}$ equals 310µN is the required force to bend the free end and move back. It can be obtained by simulation in ANSYS (see Fig. 10b).

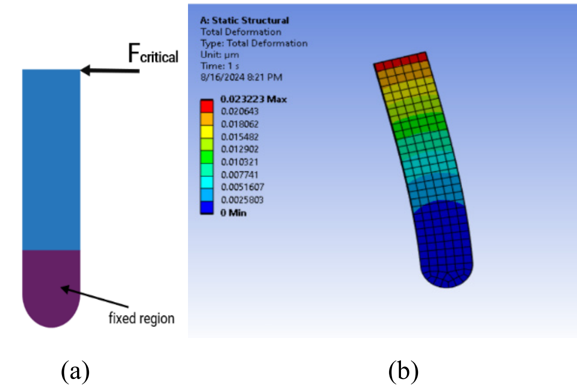

(a) (b)

Fig. 10. Critical force loads on the tip of V-beam (a); deformation of tip of the V-beam (b)

In other words, to bend the free end of V-beam, the returning force on each side F'_{re} must be satisfied with the condition as below:

$$F'_{re} = F_{critical} \quad (23)$$

From equations (20), (21) and (23), we have:

$$F_e' + 2F_{spr} + F_b = 2F_{critical} \quad (24)$$

or:

$$\frac{n' b\varepsilon\varepsilon_0 {V_{13}}^2}{g_0} + \left(2K_{spr} + \frac{4Ebw^3}{L^3}\right)\Delta x = 620 \quad (25)$$

From (25), we find out the relationship between the voltage for returning period and displacement Δx:

$$V_{13} = \sqrt{\frac{g_0\left[620 - \left(2K_{spr} + \frac{4Ebw^3}{L^3}\right)\Delta x\right]}{n'b\varepsilon\varepsilon_0}} \quad (26)$$

Fig. 11 illustrates the necesarry voltage for returning period with the change of displacement Δx from 8 to 40 µm (i.e. from one to five pitches of ratchet tooth). The minimum returning voltage V_{13min} is 24.3 (V) when the displacement reaches the value of 40µm (equals to 5 pitches of ratchet tooth), and the maximum required voltage V_{13max} = 122.73 (V) when the displacement equals only one pitch of ratchet tooth.

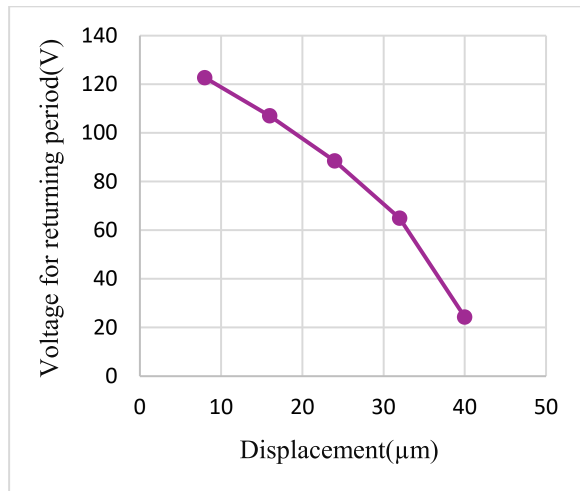

Fig. 11. The relationship between voltage V_{13} for returning period and the displacement Δx.

3. Simulation

The finite element analysis (FEA) is performed by ANSYS to confirm the calculation results and test strength condition of elastic elements such as beams, springs or *V*-beam of the self-locking mechanism. Simulation results at V_{12} equals 100 (V) are shown in Fig. 12 including the elastic force of the *V*-beams. The displacement of the shuttle Δx is 33.12 µm (Fig. 12a); the maximum stress of the actuator's beams as well as of the springs is about 230.55 MPa and 166.37 MPa, respectively (Figs. 12b and 12c).

Furthermore, the stress distribution on the *V*-beams was also derived by simulation. The result of stress distribution on the *V*-beam (when the displacement of the shuttle Δx is approximately 7.8 µm) is shown in Fig. 13.

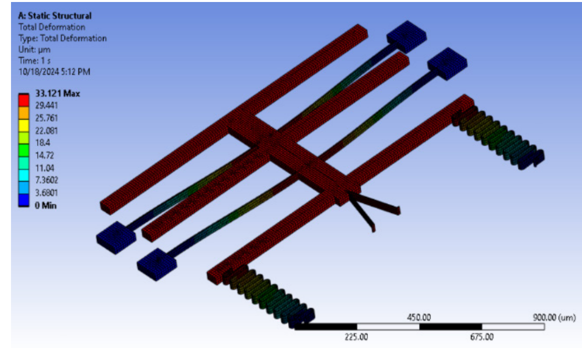

(a)

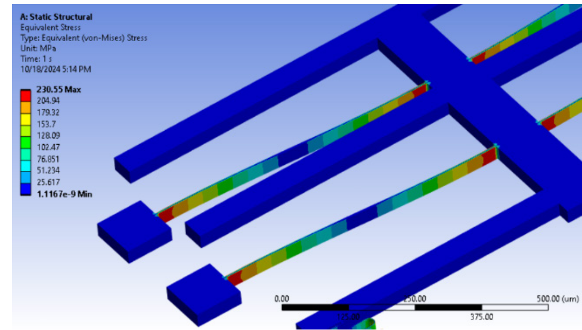

(b)

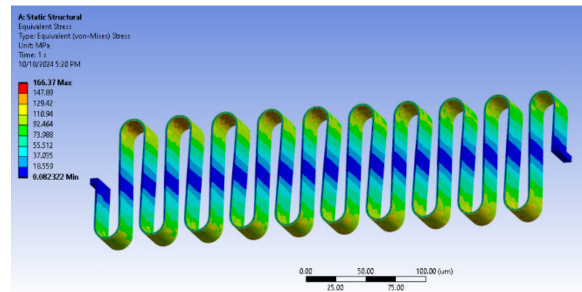

(c)

Fig. 12. Simulation result at V_{12} = 100 volt: displacement (a); maximum stress of the actuator's beam (b); stress distribution on the springs (c)

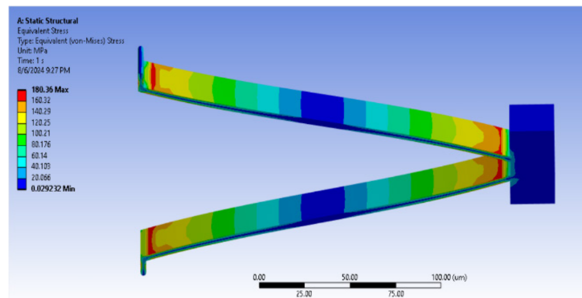

Fig. 13. Stress distribution on the *V*-beams at displacement Δx equals 7.8µm

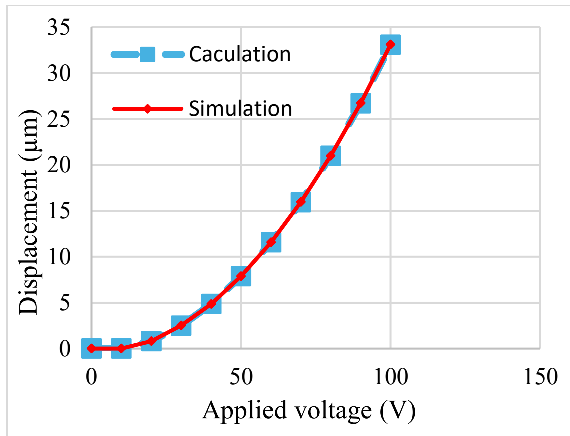

Fig. 14. Calculation and simulation of the jaw's displacement

Fig. 14 shows the calculation and simulation results of jaw's displacement with the change of the driving voltage V from 0 to 100 volt.

At the same voltage, average deviation of displacement between the calculation and simulation is only 0.3%. The maximum error is approximately 1.23% at voltage V_{12} equals 100 volts. This remaining deviation can be explained by ignoring the friction between the springs ⑥ and the substrate while compressed.

4. Conclusion

Design, force analysis, and finite element simulation of the electrostatic microgripper with new self-locking mechanism were presented in this paper. The main advantage of this structure is the integration of the simple self-locking structure that allows easy pick-and-place of micro samples without applying voltage. The displacement and stress distribution of elastic elements were also analyzed using ANSYS simulation.

Calculation result show that microgripper can obtain maximum displacement of 40µm for each side at the driving voltage of 110.06 volt.

The self-locking microgripper can be used in micro assembling or in micro robot systems to grasp, move, as well as locate exactly the position of micro samples.

References

[1] Ai Wenji, Xu Qingsong. Overview of flexure-based compliant microgrippers, Advances in Robotics Research, vol. 1, iss.1, pp. 1-19, Jan. 2014. https://doi.org/10.12989/arr.2014.1.1.001

[2] Che-Min Lin, Chen-Hsien Fan, and Chao-Chieh Lan, A shape memory alloy actuated microgripper with wide handling ranges, in 2009 IEEE/ASME International Conference on Advanced Intelligent Mechatronics, Singapore, Jul. 2009, pp. 12-17. https://doi.org/10.1109/AIM.2009.5230045

[3] Qingsong Xu, Adaptive discrete-time sliding mode impedance control of a piezoelectric microgripper in IEEE Transactions on Robotics, vol. 29, iss. 3, Jun. 2013, pp. 663-673. https://doi.org/10.1109/TRO.2013.2239554

[4] Zhang Ran, Jinkui Chu, Haixiang Wang and Zhaopeng Chen, A multipurpose electrothermal microgripper for biological micro-manipulation, Microsystem Technologies, vol. 19, pp. 89–97, Jun. 2012. https://doi.org/10.1007/s00542-012-1567-0

[5] Khan Fahimullah, Shafaat A. Bazaz, and Muhammad Sohail, Design, implementation and testing of electrostatic SOI MUMPs based microgripper, Microsystem Technologies, vol. 16, pp. 1957–1965, Aug. 2010. https://doi.org/10.1007/s00542-010-1129-2

[6] William C. Tang *et al.,* Electrostatic-comb drive of lateral polysilicon resonators, Sensors and Actuators A: Physical, vol. 21, iss. 1-3, pp. 328-331, Feb. 1990. https://doi.org/10.1016/0924-4247(90)85065-C

[7] Kim Keekyoung, *et al.,* Nanonewton force-controlled manipulation of biological cells using a monolithic MEMS microgripper with two-axis force feedback, Journal of Micromechanics and Microengineering, vol. 18, no. 5, Apr. 2008. https://doi.org/10.1088/0960-1317/18/5/055013

[8] Wierzbicki R., *et al.,* Design and fabrication of an electrostatically driven microgripper for blood vessel manipulation, Microelectronic Engineering, vol. 83, iss. 4-9, pp. 1651-1654, Apr-Sep. 2006. https://doi.org/10.1016/j.mee.2006.01.110

[9] Kalaiarasi, A. R., and S. Hosimin Thilagar, Design and modeling of electrostatically actuated microgripper in Proceedings of 2012 IEEE/ASME 8th IEEE/ASME International Conference on Mechatronic and Embedded Systems and Applications, Suzhou, China, 08-10 Jul. 2012. https://doi.org/10.1109/MESA.2012.6275528

[10] Jia Yukun, Minping Jia, and Qingsong Xu, A dual-axis electrostatically driven MEMS microgripper, International Journal of Advanced Robotic Systems, vol. 11, iss. 11, pp. 187-196, Nov. 2014. https://doi.org/10.5772/59677

[11] Yongcun Hao, *et al.*, Rotatory microgripper based on a linear electrostatic driving scheme, Microelectronic Engineering, vol. 248, Aug. 2021. https://doi.org/10.1016/j.mee.2021.111601

[12] Millet Olivier, *et al.*, Electrostatic actuated micro gripper using an amplification mechanism, Sensors and Actuators A: Physical, vol. 114, iss. 2-3, pp. 371-378, Sep. 2004. https://doi.org/10.1016/j.sna.2003.11.004

[13] Chen Brandon K., Yong Zhang, and Yu Sun, Active release of micro-objects using a MEMS microgripper to overcome adhesion forces in Journal of Microelectromechanical Systems, vol. 18, iss. 3, Jun. 2009, pp. 652–659. https://doi.org/10.1109/JMEMS.2009.2020393

[14] Guangmin Yuan, *et al.,* A microgripper with a post-assembly self-locking mechanism, Sensors, vol. 15, iss. 8, pp. 20140-20151, Aug. 2015. https://doi.org/10.3390/s150820140

[15] Hwang Il-Han, Yong-Gu Lee, and Jong-Hyun Lee, A micromachined friction meter for silicon sidewalls with consideration of contact surface shape, Journal of Micromechanics and Microengineering, vol. 16, no. 11, 2006.